Nonlinear Analysis of Microwave Superconductor Devices Using Full-Wave Electromagnetic Model

Mohamed A. Megahed, *Member, IEEE*, and Samir M. El-Ghazaly, *Senior Member, IEEE*

Abstract— **This paper presents a full electromagnetic wave analysis for modeling the nonlinearity in high temperature superconductor (HTS) microwave and millimeter-wave devices. The HTS nonlinear model is based on the Ginzburg-Landau theory. The electromagnetic fields associated with the currents on the superconducting structure are obtained using a three-dimensional full wave solution of Maxwell's equations. A three-dimensional finite-difference time-domain algorithm simultaneously solves the resulting equations. The entire solution is performed in time domain, which is a must for this type of nonlinearity analysis. The macroscopic parameters of the HTS, the super fluid penetration depth and the normal fluid conductivity, are calculated as functions of the applied magnetic field. The nonlinear propagation characteristics for HTS transmission line, including the effective dielectric constant and the attenuation constant, are calculated. As the power on the transmission line increases, the phase velocity decreases and the line losses increase. The nonlinearity effects on the current distributions inside the HTS, the electromagnetic field distributions, and the frequency spectrum are also analyzed.**

I. Introduction

THE DISCOVERY of high temperature superconductor (HTS) in 1986 paved the way for a new exciting technology which is not mature yet. These HTS materials have potential applications for passive microwave and millimeter-wave devices. They acquire better performance than normal conductors with respect to low loss, dispersion, low noise, high sensitivity, and higher frequency of operation. The workhorse HTS materials are yttrium-based YBCO with superconducting transition temperature of 90 K, and thallium-based (TBCCO) with superconducting transition temperature over 100 K. The use of HTS in microwave and millimeter-wave devices presents new challenges which are not relevant in the design of normal metal devices. The field penetration effects on the device performance need to be taken into consideration [1]. To exploit the exciting characteristics of HTS materials, accurate and flexible models have to be developed. London equations are simultaneously solved with Maxwell's equations to predict the performance of the HTS used in microwave and millimeter-wave devices [2]–[8]. Despite the usefulness and simplicity of this approach, this model may be only applied for low power applications. Moreover, the high current value existing in some applications may not exceed the high temperature superconductor critical current densities of high-quality YBCO films, but they are high enough to drive the HTS into nonlinear behavior. As an example, HTS transmission line resonators in narrow band filters have high peak current densities, which result from the high standing-wave ratios on the resonator lines [9]. The nonlinear characteristics of the HTS result in generation of harmonics and also spurious products created by the mixing of multiple input signals. Better understanding for the dependence of the penetration depth inside the superconducting material as well as the superconductor electron density on the microwave magnetic field requires a rigorous nonlinear model. This model must only be developed in time-domain and never in the frequency domain or phasor form of fields [10].

The problem of modeling the nonlinearity in HTS microwave and millimeter has been tackled before using different approaches. An iterative method combining the spectral domain approach and the impedance boundary condition model is applied in [11] and [12]. The Ginzburg-Landau (GL) theory was used to predict the nonlinear behavior in a superconducting stripline resonator as a function of the input current [13]. These approaches were based on frequency domain calculation. A macroscopic model of the nonlinear constitutive relations in superconductors is derived from a velocity distribution assumption [14]. To our knowledge, modeling and full-wave analysis of the nonlinearity associated with microwave HTS devices were never performed in the time domain.

In this paper, a nonlinear full-wave solution, based on the GL theory is developed using the finite-difference time-domain (FDTD) technique. The GL theory is independent of the microscopic mechanism in superconductor and is purely based on the ideas of the second order phase transition only. The physical characteristics of the HTS are blended with the electromagnetic model using the phenomenological two fluid model. Maxwell's and GL equations are solved simultaneously in three-dimensions. This time-domain nonlinear model is successfully used to predict the effects of the nonlinearity on the performance of HTS transmission lines. This approach takes into account the field penetration effects. The spatial distribution of the total electrons and the number of the super electrons compared to the normal electrons vary with the applied power. A study of the nonlinearity effects on the propagation characteristics, current distributions, electromagnetic field distribution, and frequency spectrum is conducted. Our model is flexible and can be used for any of the planar microwave and millimeter-wave devices that include HTS material. This approach is not only useful to predict

Manuscript received January 13, 1995; revised August 1, 1995. This work was supported by the National Science Foundation Grant ECS-9108933.

The authors are with the Department of Electrical Engineering, Telecommunications Research Center, Arizona State University, Tempe, AZ 85287-5706 USA.

IEEE Log Number 9414851.

the nonlinearity effects on microwave devices performance but also can be utilized in the characterization of the HTS materials.

II. Time-Domain Versus Frequency-Domain Numerical Techniques

Numerical characterizations and modeling of guided-wave components has been an important research topic in the past three decades. When a specific structure is analyzed, one has to make a choice which method is best suited for the structure. Obviously, the choice may not be unique. One must make a critical assessment for every possible method. Analysis and modeling the nonlinearity imposes some restrictions one the selected numerical techniques. It is known that the application of a signal to a wave-guiding structure including nonlinear material causes frequency mixing to occur. This results in generation of harmonics and spurious products. The frequency domain approach is based on analysis in the Fourier transform domain. It provides an elegant tool for the reduction of the partial differential equations of mathematical physics into ordinary ones, which in many cases are amenable to further analytical processing. The time-dependent partial differential equation is decoupled into a series of frequency-dependent ones. Hence, the solution is separately carried on each frequency component. The time-domain solution can be obtained by the superposition of the results calculated at each frequency components. This approach is widely used in problem containing linear materials. However, when a nonlinear material is used, the partial differential equation can not be transformed to the frequency domain. The equations for the various harmonics are no longer separable, and the superposition technique is not allowed. Hence, the equations must be solved in time domain. One should notice that this is a fundamental issue. It is not a matter of approximation or simplification.

III. Nonlinear Superconducting Model

A. Theory

The macroscopic electromagnetic London's equations are able to account satisfactorily for the current persistence and the magnetic flux exclusion (Meissner) effect [15]. However, they do not give a completely satisfactory macroscopic picture of all superconducting phenomena in a magnetic field, because they regard the superconducting material as being entirely superconducting or entirely normal. These deficiencies were overcome in 1950 by Ginzburg and Landau, who proposed a phenomenological set of equations, allowing for spatial variations in the superconducting order due to the presence of a magnetic field. The correctness of GL equations have been proved by Gorkov based on the microscopic theory for conventional superconductor materials, and extended beyond their region of validity by other researchers [16]. However, an exact theory describing the new HTS does not seem available.

The construction of GL theory is independent of the microscopic mechanism and is purely based on the ideas of the second order phase transition only. GL began their argument by introducing a quantity to characterize the degree of superconductivity at various points in the material. This quantity is called the "order parameter" and denoted by $\psi(\bar{r})$. The order parameter is defined to be zero for a normal region and unity for a fully superconductor region at zero temperature with zero magnetic field. Clearly, $\psi(\bar{r})$ must be closely related to the super fluid fraction in a two-fluid model, but the two quantities are not chosen identical. Rather, to allow for supercurrent flow, $\psi(\bar{r})$ is taken as a complex function and interpreted as analogous to a "wave function" for superconductivity, so that its magnitude square can be identified with the super fluid density $N_s(\bar{r})$

$$N_s(\bar{r}) = |\psi(\bar{r})|^2. \tag{1}$$

It should be noted that ψ is not the system wave function for the electrons in the material, since it is defined to be zero in the normal state. However, pursuing the interpretation of the order parameter as a wave function, it is reasonable to write the expression for the supercurrent $\bar{J}_s$, in the absence of a magnetic field, as

$$\bar{J}_s = \frac{e^*}{2m^*}[\psi^*(\bar{r})\frac{\hbar}{i}\nabla\psi(\bar{r}) + \psi(\bar{r})\frac{\hbar}{i}\psi^*(\bar{r})] \tag{2}$$

where e^* and m^* are the charge and mass of the entities whose wave function is $\psi(\bar{r})$, $\hbar$ is the reduced Plank's constant, and i is $\sqrt{-1}$. It is equally natural to include the magnetic field via the vector potential $\bar{A}$

$$\bar{J}_s = \frac{e^*}{2m^*}\left[\psi^*(\bar{r})\left(\frac{\hbar}{i}\nabla - e^*\bar{A}(\bar{r})\right)\psi(\bar{r}) + \psi(\bar{r})\left(\frac{\hbar}{i}\nabla - e^*\bar{A}(\bar{r})\right)\psi^*(\bar{r})\right]. \tag{3}$$

From the two-fluid hydrodynamic model point of view, the super fluid component has been regarded as a "quantum fluid" and a quantum wave function is associated with it. Reinforcing this interpretation, a more suggestive form of (3) is

$$\bar{J}_s(\bar{r}) = e^* N_s(\bar{r})\bar{\nu}_s(\bar{r}) \tag{4}$$

where $\nu_s(\bar{r})$ is the super fluid velocity, and can be related to the phase of the order parameter

$$\bar{\nu}_s(\bar{r}) = \frac{1}{m^*}\left[\hbar\nabla\frac{\psi(\bar{r})}{|\psi(\bar{r})|} - e^*\bar{A}(\bar{r})\right]. \tag{5}$$

Furthermore, if there is no position dependence to the superconductivity and the order parameter $\psi(\bar{r})$ is independent of position $\bar{r}$, then (3) reduces to the London's relation

$$\bar{J}_s(\bar{r}) = \frac{e^{*2}}{m^*}N_s\bar{A}(\bar{r}). \tag{6}$$

Next, a relation determining ψ must be constructed. Ginzburg and Landau focused on the free energy of the material F_s, which they *assume* as a functional of ψ and ψ^*. The equation determining ψ is obtained by requiring that F_s, be a minimum with respect to variations of ψ^*. The condition that F_s, be a minimum can be shown to be equivalent to requiring that the super fluid and normal components of the two-fluid model be in stable equilibrium with respect to each other. Thus, the functional F_s, plays a role analogous

to a Lagrangian of Schrodinger wave mechanics, while its minimum value with respect to ψ and ψ^* is just the free energy of the superconducting phase in thermodynamic equilibrium with the magnetic field.

GL phenomenological theory results in a set of two equations relating the order parameter ψ and the magnetic vector potential $\overline{A}$. These equations can be reduced to a dimensionless form by taking all the lengths in units of the weak-field penetration depth λ, measuring the magnetic field in terms of the thermodynamic critical magnetic field H_c, and introducing a reduced order parameter normalized by its zero-field position-independent value. Then, the dimensionless GL equations can be expressed as follows

$$\nabla \times \overline{H}_N = \frac{1}{2i}\left[\psi_N^*\left(\frac{1}{i\kappa}\nabla_N - \overline{A}_N\right)\psi_N + \psi_N\left(-\frac{1}{i\kappa}\nabla_N - \overline{A}_N\right)\psi_N^*\right] \tag{7}$$

$$(1-\psi_N^2)\psi_N - \left(\frac{1}{i\kappa}\nabla_N - \overline{A}_N\right)^2\psi_N = 0. \tag{8}$$

The subscript N denotes normalized quantities. The boundary conditions for $\overline{A}_N$ and ψ_N at the superconductor-insulator interface are given by

$$\hat{n}\cdot\left(\frac{1}{i\kappa}\nabla_N - \overline{A}_N\right)\psi_N = 0 \tag{9}$$

$$\hat{n}\times(\nabla_N \times \overline{A}_N) = \hat{n}\times\mu_0\overline{H}_N. \tag{10}$$

Equation (9) forces the normal component of the conduction current to vanish at superconducting-insulator boundary, resulting the boundary condition for the order parameter ψ. Equation (10) indicates that the boundary conditions imposed on the magnetic vector potential $\overline{A}$ corresponds to the magnetic field tangential to the superconductor surface. The dimensionless parameter κ, known as GL parameter is defined as

$$\kappa = \sqrt{2}(e^*/\hbar)\mu_0 H_c \lambda_L^2 \tag{11}$$

where

$$\lambda_L = \sqrt{m^*/\mu_0 e^{*2}\psi_\infty^2}$$
$$|\psi_\infty|^2 = n_L^*$$
$$\overline{H}_N = \overline{H}/H_c$$
$$\overline{A}_N = \overline{A}/\lambda_L\mu_0 H_c$$
$$\nabla_N = \lambda_L\nabla$$
$$\psi_N = \psi/\psi_\infty$$

λ_L and n_L^* are the low field London penetration depth and the low field superconducting electron density. The subscript N will be omitted in the rest of the paper, for simplicity.

A common feature of the family of HTS, including YBaCuO and TlBaCaCuO, is that they all have layered crystal structures. It is generally believed that the two-dimensional CuO_2 network is the most essential building block of the HTS materials [17]. This means that we must take account of the strong anisotropy of the new HTS systems, and the GL type scheme needs to be modified [18]. The anisotropy in HTS materials is a complicated issue, which we analyzed fully in a separate paper [19]. However, thin-film microwave transmission lines will favor films in which conducting sheets lie in the plane of the film. To overcome the limitation in applying the GL theory to the new HTS materials, the solution for GL equations is only performed for the longitudinal super fluid z-current component in the HTS strip. The transverse x- and y-current components are calculated using London low field model since the current in the transverse plane is relatively small for most of microwave and millimeter-wave applications working in the low gigahertz band. Using the London gauge $\nabla\cdot\overline{A} = 0$ and assuming $\psi = |\psi|\exp(i\theta)$, the normalized GL equations for the super fluid z-component current density can be simplified to the following expressions

$$\nabla_t^2 A_z = |\psi|^2 A_z \tag{12}$$

$$\frac{1}{\kappa^2}\nabla_t^2|\psi| = |\psi|\left(|\psi|^2 - 1 + \frac{A_z^2}{2}\right) \tag{13}$$

where t stands for the transverse x–y direction and $\nabla_t\theta = 0$. The required boundary conditions become

$$\hat{n}\times(\nabla_t\times\hat{z}A_z) = \mu_0\overline{H}_t \tag{14}$$

$$\hat{n}\cdot\nabla_t|\psi| = 0. \tag{15}$$

B. Solution of GL Equations

The GL coupled nonlinear differential equations are solved simultaneously to obtain the superconducting current and the order parameter. The first nonlinear GL equation, which resolves the order parameter, is solved using a Newton-SSOR iteration scheme. The second GL equation, which corresponds to the superconducting current, is manipulated using a linearized scheme. These two equations are solved iteratively until convergence, starting with initial conditions $|\psi| = 1$ and $A_z = 0$. The described procedure is rapid and robust, and is successfully applied to the solution of GL equations both in one- and two-dimensions. The solution converges in few iterations, which depends on the applied magnetic field intensity.

In our analysis, the HTS macroscopic parameters are those measured for $YBa_2Cu_3O_{7-x}$ at $T = 77$ K with T_c equals to 90 K. The GL parameter κ equals to 44.8. The corresponding penetration depth $\lambda(T)$ and critical magnetic flux density $\mu_0 H_c(T)$ equals to .323 μm and 0.1 T, respectively. Fig. 1 presents the variations of the super fluid current density with distance for one-dimensional superconducting slab at different magnetic fields. These results are in excellent agreement with those in Lam *et al.* [13]. The nonlinearity in the superconducting material is clear, especially near the edge of the material. The superconducting current near the edge is suppressed in favor of the normal fluid current, which explains the increase in the losses as the applied field increases. Also, the predicted penetration depth using GL theory is higher than the low-field value calculated from the linear London model, which can explain the more pronounced slow wave effects associated with the superconducting material as the magnetic field intensity increases. Thus, the field penetration effects on the superconducting material is represented more rigorously

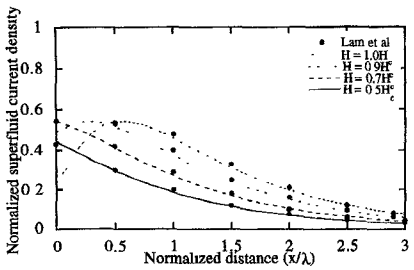

Fig. 1. Normalized super fluid current density in $YBa_2Cu_3O_{7-x}$ HTS slab.

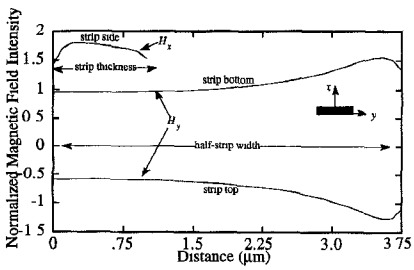

Fig. 2. Tangential magnetic field intensity to a $YBa_2Cu_3O_{7-x}$ HTS strip in microstrip line.

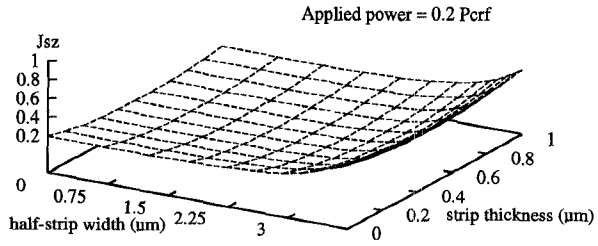

Fig. 3. Normalized super fluid current density distribution in $YBa_2Cu_3O_{7-x}$ HTS strip in microstrip line (applied power $= 0.2P_{\rm crf}$).

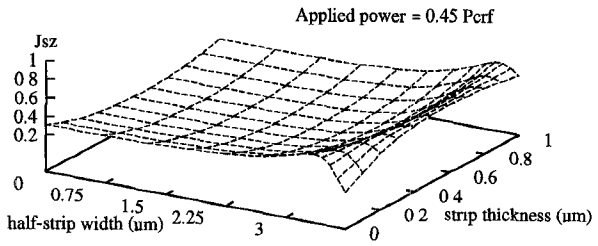

Fig. 4. Normalized super fluid current density distribution in $YBa_2Cu_3O_{7-x}$ HTS strip in microstrip line (applied power $= 0.45P_{\rm crf}$).

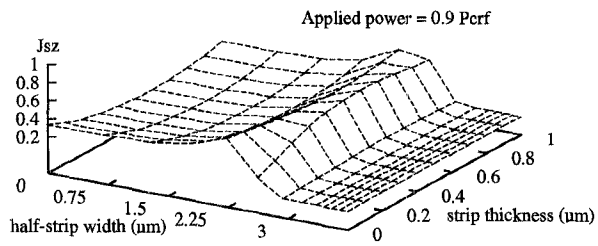

Fig. 5. Normalized super fluid current density distribution in $YBa_2Cu_3O_{7-x}$ HTS strip in microstrip line (applied power $= 0.9P_{\rm crf}$).

in the GL theory compared to London model. These results confirm the success of the phenomenological GL model to get a field and position dependent macroscopic parameters for the superconducting material.

To demonstrate the versatility of this scheme, two-dimensional solution for a typical HTS strip used in microwave and millimeter-wave devices is presented. The strip width and thickness are 7.5 and 1.0 μm, respectively. The strip is divided into a numerical grid cells. The generated mesh is uniform in the vertical direction and nonuniform in the horizontal direction. The horizontal mesh size decreases near the edges of the strip where more rapid change in the macroscopic parameters of the superconductor is expected. The mesh size is chosen smaller than the low-field penetration depth. The HTS parameters are the same as previously described. The typical tangential magnetic field shown in Fig. 2 is applied to the strip. This field distribution is obtained for the HTS microstrip line using a full-wave electromagnetic simulator, which will be explained later. The corresponding applied power is calculated. GL equations are solved at different levels of applied power. The maximum rf power $P_{\rm crf}$, where the HTS microstrip looses completely its superconductivity, is predicted. Its value equals to 920 W/cm^2. The normalized superconducting current distributions are shown in Figs. 3–5 for different applied power levels: 834, 410, and 181.8 W/cm^2 denoted by 0.9, 0.45, and $0.2P_{\rm crf}$, respectively. Fig. 3 shows that the HTS may be considered linear when the applied magnetic field is low, i.e. approximately less than $0.2P_{\rm crf}$. As the applied power increases, the dependence of the macroscopic parameter of the superconducting material on the magnetic field becomes nonlinear. A typical distribution for the normalized superconducting current density in this nonlinear region at $0.45P_{\rm crf}$ is presented in Fig. 4. London's equation fails to predict the superconductor behavior in this nonlinear region, even the type II superconducting material is still in the mixed state, and possesses a relatively good superconductor nature. Fig. 5 demonstrates that the superconducting material partially looses its superconductivity at high rf power $0.9P_{\rm crf}$. It is obvious that the material lost its superconductivity near the edge of the strip where the singularity in the field is expected. On the other hand, the material behaves as a good superconductor at the center of the strip. This behavior will not only introduce nonlinearity effects but it will also increase the noise. Fig. 6 presents the normalized super fluid electron density at $0.45P_{\rm crf}$. It is clear that the bottom part of the strip looses its superconductivity much faster than the top section. This can be explained by the effect of the dielectric substrate underneath the strip, which increases the field intensity at the bottom side. Thus, superconducting applications will favor low dielectric substrate to decrease the nonlinearity effects in microwave and millimeter-wave applications.

IV. Time-Domain Electromagnetic Model

The FDTD solution of Maxwell's equations is one of the most suitable numerical modeling approaches for the electromagnetic analysis of volumes containing arbitrary shaped dielectric and metal objects. FDTD is relatively simple in

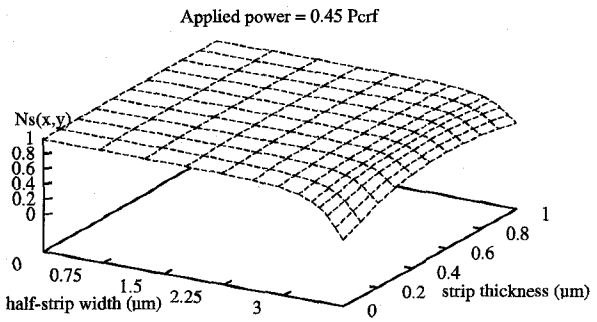

Fig. 6. Normalized super fluid electron density distribution in $YBa_2Cu_3O_{7-x}$ HTS strip in microstrip line (applied power = $0.45P_{crf}$).

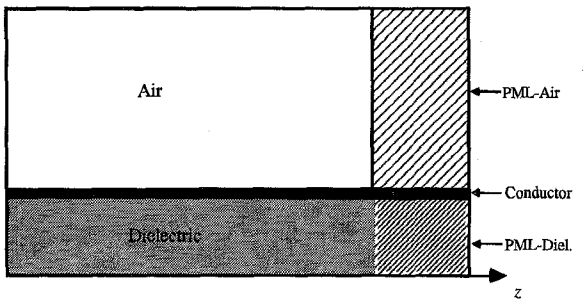

Fig. 7. Microstrip line with the perfectly matched layers (PML) absorbing boundaries.

concept and execution. However, it is remarkably robust, and provides highly accurate modeling predictions for a wide variety of electromagnetic wave interaction problems [20]–[22]. FDTD is a marching-in-time procedure which simulates the continuous actual waves by sampled-data numerical analogs propagating in a computer data space. The FDTD is well known [23]. Therefore, it is not discussed here. Only interesting features peculiar to our approach will be presented. These features are necessary to successfully model the HTS microwave devices, where the field penetration effects need to be taken into consideration. They are the nonuniform graded mesh generator [8], the Perfectly Matched Layer Absorbing Boundary Conditions (PML-ABC) [24], and the execution of the computer code on Massively Parallel Processors machine (MPP) [25].

The developed three-dimensional finite-difference time-domain scheme is capable of modeling the finite thickness of the HTS strip. No approximations are made to the strip thickness. This leads to a very dense uniform mesh that requires a non realistic memory storage. To alleviate this problem, a graded nonuniform mesh generator is implemented along the cross section of the waveguiding structure. The computational domain is discritized according to the following expression

$$\Delta x(i)_{i=1}^{i=n} = W * \left[\left(\frac{i}{n}\right)^p - \left(\frac{i-1}{n}\right)^p\right] \qquad (16)$$

where Δx is the mesh size, W distance to be discritized, n number of points, and p is the mesh resolution factor. The smallest mesh size is chosen inside and around the HTS strip. It is equal to a fraction of the magnetic field penetration depth for the HTS material. The mesh resolution factor p must be optimized to minimize the dispersion introduced by the nonuniform discretization. The Courant stability condition is based on the smallest mesh size.

The computational domain is closed by the PML-ABC. This approach provides a termination for the FDTD scheme with negligible reflection using a non-physical lossy medium adjacent to the outer boundary. In our FDTD scheme, the mesh is terminated by extending the dielectric layers into its matching PML [26]. The conductors are extended without PML region. This configuration, shown in Fig. 7, simulates an extremely lossy waveguiding structure. The propagating wave is highly attenuated in the PML without any reflection at the interface between the PML and the actual structure. This approach fits the need for an appropriate ABC for dispersive multimodal propagation. It is essential for calculating the dispersion characteristics of a transmission line, especially the losses. The enhancement applied to the PML-ABC approach eliminates any possible discontinuity effects at the end of the line.

Recent advances in FDTD modeling concepts and software implementation, combined with advances in computers, have expanded the scope, accuracy, and speed of FDTD approach. FDTD technique has an explicit or semi-implicit scheme, where parallel computers provide a good environment to run such schemes [27]. The $\overline{E}$ and $\overline{H}$ fields components are calculated using their nearest $\overline{H}$ and $\overline{E}$ field components. This algorithm avoids the time consuming communication within the MPP. The size of the problem must be optimized to efficiently use the parallel machine. The fields arrays are expected to be exactly mapped and properly aligned on the parallel processors to get the maximum computational capacity of the MPP. The computer code for our analysis is written in FORTRAN 90 and is executed in massively parallel machine (MASPAR) environment. The implementation of the PML-ABC in three dimension requires splitting each field components into two subcomponents. This algorithm requires a large memory storage on parallel machine. However, the computational gains acquired by using both the PML-ABC and the MPP are indispensable for completing this project.

The time dependence of the excitation is chosen as a Gaussian pulse. The turn-on amplitude of the excitation ought to be small and smooth. The field patterns of the appropriate modes, which are obtained from an exhaustive time simulation, is enforced on the source plane. After the excitation pulse is launched, the PML-ABC is switched at the front wall. The Gaussian pulse width is chosen to reduce the discretization errors, especially with nonuniform mesh. The maximum spatial step size is less than $\frac{1}{40}$ of the smallest wavelength existing in the excitation pulse. A perfectly magnetic wall is inserted at the line of symmetry of the transmission line. The simulation is performed on half the structure. The ground plane is considered as a perfect conductor, for simplicity. Two probes along the transmission line are used to record the time dependent field components. The propagation characteristics of the HTS transmission line as functions of frequency are calculated by taking the Fourier transform of those field

components [21]. Our electromagnetic simulator is validated and the results are presented in [19].

V. Nonlinear 3-D Full-Wave HTS Model

The nonlinear superconducting model is incorporated into the 3-D full-wave electromagnetic simulator using the two fluid model postulate. The two fluid model assumes that the electron gas in a superconductor material consists of two gases, the superconducting electron gas and the normal electron gas [29]. The main macroscopic parameters of the superconducting material are the penetration depth λ_s and the normal conductivity σ_n. The physical nature of the superconducting phenomena is included in the dependence of the charge carrier densities and the effective masses of the superconducting and normal states, as well as the normal electrons relaxation time, on the temperature. The total current density in superconducting material is expressed as follows

$$\overline{J} = \overline{J}_n + \overline{J}_s \tag{17}$$

where $\overline{J}_n$ is the normal state current density, which obeys Ohm's law

$$\overline{J}_n = \sigma_n(H(\overline{r}), T)\overline{E} \tag{18}$$

and $\overline{J}_s$ is the superconducting fluid current density, which follows the modified form of GL equation

$$\frac{\partial \overline{J}_s}{\partial t} = \frac{1}{\mu_0 \lambda_s^2(H(\overline{r}), T)}\overline{E}. \tag{19}$$

Here, the HTS macroscopic parameters σ_n and λ_s are nonlinear and are assumed to be field and temperature dependent. The temperature dependence is approximated by the well-known Gorter-Casimir model. In fact, this model is in good agreement with the measured penetration depth for conventional superconductors, but not for HTS [30]. The field dependence is obtained from the solution of the phenomenological GL equations. The normalized order parameter, which corresponds to the fraction of the super fluid electrons density and is shown in (11), is calculated. It is field, position, and temperature dependent. The normal fluid electrons density is calculated from the conservation of the total number of electrons in the superconductor. The spatial, field, and temperature dependent magnetic field penetration depth λ_s for the superconductor is obtained from the following expressions

$$\lambda_s(H(\overline{r}), T) = \frac{\lambda_s(0,0)}{\sqrt{\left(\frac{\psi(H(\overline{r}), T)}{\psi(0,T)}\right)^{\alpha} * \left(1 - \left(\frac{T}{T_c}\right)^{\beta}\right)}} \tag{20}$$

where $\lambda_s(0,0)$ is the low field penetration depth measured at $T = 0$ and $H = 0$ and T_c is the critical temperature for the superconductor calculated at $H = 0$. The parameters α and β may be obtained from experimental studies. In our analysis, we chose $\alpha = 2$ and $\beta = 4$ following GL model for the field dependence and Gorter-Casimir for the temperature approximations. The corresponding normal conductivity is expressed as follows

$$\sigma_n(H(\overline{r}), T) = \sigma_n(H_c/T_c) \cdot \left[1 - \left(\frac{\psi(H(\overline{r}), T)}{\psi(0,T)}\right)^{\alpha} * \left(1 - \left(\frac{T}{T_c}\right)^{\beta}\right)\right] \tag{21}$$

where $\sigma_n(H_c/T_c)$ is the maximum normal conductivity measured either at $T = T_c$ or $H = H_c$ and H_c is the critical magnetic field for the superconductor calculated at $T = 0$. Equations (20) and (21) are one of the main results of this paper.

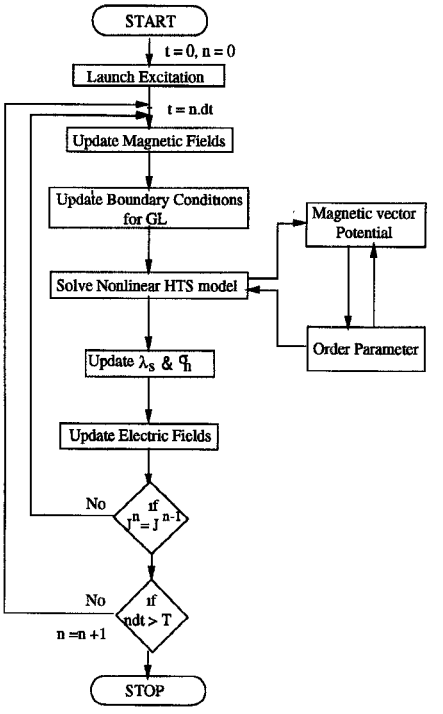

Fig. 8. Flow chart of the nonlinear analysis algorithm.

Our nonlinear analysis algorithm can be summarized in Fig. 8. First, the excitation pulse is launched into the HTS microwave device. Then, the magnetic field components are updated using the FDTD approach. Next, the tangential magnetic field to the HTS strip surface are used as boundary conditions for the nonlinear HTS simulator. The normalized super fluid electrons density is calculated as previously described. The spatial, field, and temperature dependent macroscopic HTS parameters σ_n and λ_s are updated. The super fluid and normal fluid current densities are calculated. Finally, the electric field components are updated using the electromagnetic simulator. This procedure is repeated for a time period suitable to analyze wave propagation characteristics inside the structure. The temporal fields are probed during the simulation process. The applied power is measured at the first probe.

VI. Results and Discussion

The results are obtained for $YBa_2Cu_3O_{7-x}$ superconducting microstrip line, shown in Fig. 9 with critical temperature

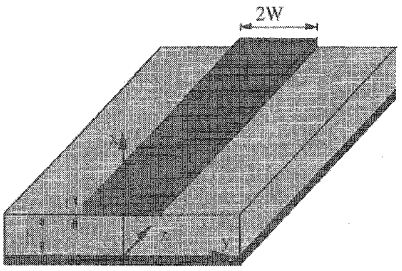

Fig. 9. HTS Microstrip line geometry.

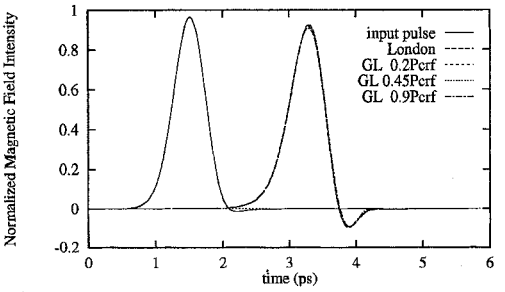

Fig. 10. Normalized tangential magnetic field intensity under the HTS strip probed at 60 and 150 μm.

of 90 K, critical magnetic flux density $\mu_0 H_c(T)$ of 0.1 T, and GL parameter of 44.8 at 77 K. The superconducting microstrip line has a 50 Ω impedance with a strip width of 7.5 μm, and a thickness of 1 μm. The substrate thickness is 10 μm with $\varepsilon_r = 13$. The transmission line characteristics are simply chosen to demonstrate the nonlinear wave propagation along the line. The maximum rf power, P_{crf}, where the HTS microstrip looses completely its superconductivity, is predicted using GL solution. Its value equals to 920 W/cm^2. Numerical results are obtained at different levels of the applied power: 834, 410, and 181.8 W/cm^2 denoted by 0.9, 0.45, and $0.2P_{\mathrm{crf}}$, respectively. The temporal magnetic field propagating along the line are probed at 60 and 150 μm, and shown in Fig. 10. The amplitude of the wave is attenuated as the applied field increases. Also, the slow wave effect can be observed from the figure. Fig. 10 also shows that London's model incorrectly predicts higher pulse amplitudes and lower attenuation even at high power. This qualitative discussion gives a good insight into the behavior of the wave propagating along the transmission line. Fig. 11 compares the effective dielectric constant of the transmission line at different applied power levels. Strictly speaking, the effective dielectric constant of the transmission line did not vary. Actually, the effective magnetic permeability of the line was changed. Hence, the propagation velocity did change with the applied power. Since the product of the electric permittivity and the magnetic permeability appear in the phase velocity calculation, variations in the phase velocity are normally expressed in terms of the effective dielectric constant. The authors acknowledge that for the case at hand, the effective permeability would be the correct presentation of the device physics. However, it was not used to avoid confusing the readers by implementing a new terminology. The effective dielectric constant predicted using London's equations is smaller than the one obtained from GL solution at low applied power. This can be explained knowing that the penetration depth predicted by London theory is smaller than the one obtained from GL model, which agrees well with the experimental observations [30]. The effective dielectric constant increases as the applied power increases. This slow wave effect is due to the increase in the internal inductance of the line introduced by the increase in the field penetration as the applied power increases. The fractional change in the effective dielectric constant at different power levels obtained from GL model with respect to the one calculated using London's theory is drawn in Fig. 12. The change in the effective dielectric constant increases with the increase in the power level up to $0.7P_{\mathrm{crf}}$. It is approximately constant for higher power levels, where almost complete field penetration occurs. The attenuation constant for the HTS at different levels of applied power is presented in Fig. 13. As the applied power increases, the attenuation constant increases as well. This can be explained by the increase in the normal electron density in favor of the super electron density as the field penetrates the HTS. Also, It is observed that the HTS loses its superconducting characteristics earlier than its static critical power. This is due to the field singularity associated with the planar microwave and millimeter-wave devices. It is noticed that the change in the propagation characteristics of the HTS microstrip line is not linear with the applied field. The change is more pronounced as the applied power increases. This is understood from the nature of the superconducting material, which deteriorates very quickly as the applied power approaches its critical value. The fractional change in the attenuation constant obtained from GL model with respect to the value predicted by London model at 10 GHz is depicted in Fig. 14. It is clear that the HTS looses its superconductivity very quickly as the applied power approaches the electromagnetic critical power. Also, the nonlinearity associated with the HTS appears very early, even with the material in fairly good superconducting stage. The change in the losses is faster and more nonlinear than the change in the phase velocity. This can be explained knowing that the losses are ohmic, which are induced by the moving particles. On the other hand, the effect on the phase velocity is a variation in the stored kinetic energy in the superconductor which is mostly a wave effect. Hence, particle related effects can be stronger and observed before the wave related effects.

The effect of the applied field on the current distribution is presented in Figs. 15–17. Fig. 15 shows the super fluid current distribution at the bottom of the HTS strip. It is observed that the London model under estimates the current carrying capacity of the HTS material. The HTS strip looses part of its superconductivity at the edges as the applied power increases from 0.2–$0.45P_{\mathrm{crf}}$. For $0.9P_{\mathrm{crf}}$ case, the partial loss of the superconductivity is induced across the entire cross section of the HTS strip. It is more pronounced at the edge of the HTS strip, where the super fluid current for the $0.9P_{\mathrm{crf}}$ case is almost equal to the $0.45P_{\mathrm{crf}}$ one. The super fluid current distribution at the top of the HTS strip is presented in Fig. 16.

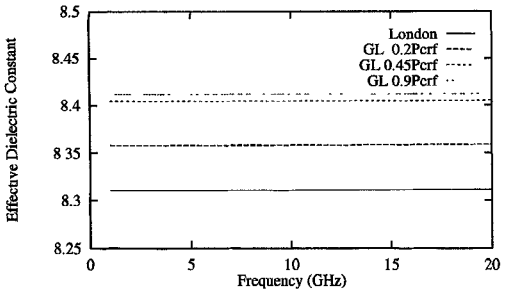

Fig. 11. Effective dielectric constant for the HTS microstrip line at different applied power levels.

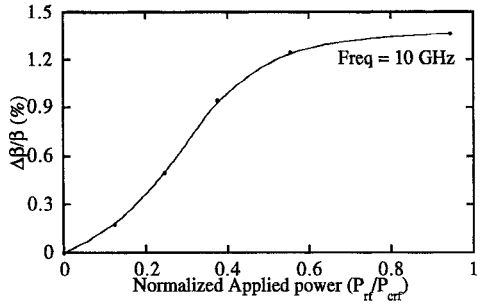

Fig. 12. Fractional change in the effective dielectric constant for the HTS microstrip line with applied power w.r.t. the linear model.

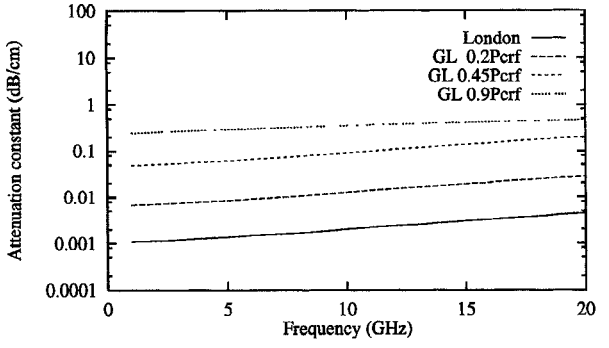

Fig. 13. Attenuation constant for the HTS microstrip line at different applied power levels.

The current values are less than the one obtained for the bottom of the strip as explained before. For the $0.9P_{\text{crf}}$ case, the super fluid current increases at the top surface because the applied field is less than the critical magnetic field of the HTS material. Thus, the superconductor redistributes the super fluid as the applied field increases. The normal fluid current density behavior will be opposite to the super fluid one based on to the conservation in the total number of electrons in the HTS. Fig. 17 shows the super fluid current distribution at the side of the HTS strip. The superconductivity of the HTS material decreases as the applied power increases. The distribution obtained from GL model at low power levels equals to the one predicted by the London model. Then, the effect of the nonlinearity on the electromagnetic field distribution in the microstrip line configuration is studied. The normalized

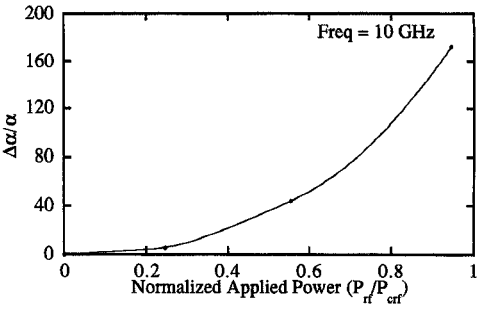

Fig. 14. Fractional change in the attenuation constant for the HTS microstrip line with applied power w.r.t. the linear model.

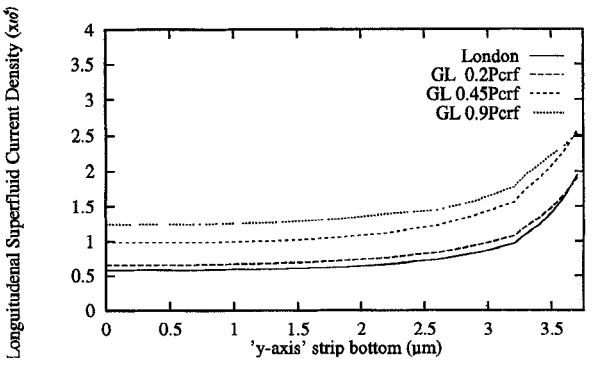

Fig. 15. Normalized longitudinal super fluid current density at the bottom surface of the HTS strip at different applied power levels.

tangential magnetic field intensity at the top and the bottom of the strip are presented in Fig. 18. The effect of the applied power on the electromagnetic field distribution is small. It is only observed near the edge of the strip. This explains the small change in the phase velocity of the wave propagating along the line. Finally, the effect of the nonlinearity on the frequency spectrum of the wave propagating along the line is analyzed in Fig. 19. The fractional change in the amplitude of the output pulse frequency components increases with the applied power. It is observed that as the power level increases, the amplitudes of the different harmonics change, which is one of the primarily characteristics of nonlinear devices. This confirms our point that the nonlinearity has to be modeled in the time domain. The results calculated from GL model for low applied power are approximately the same as the ones obtained from the linear London model. This validates our treatment for the HTS as linear material below the low applied power value.

VII. Conclusion

A nonlinear full-wave three-dimension time-domain analysis for the HTS microwave devices is presented. This approach takes into account the variation of the macroscopic parameters of the superconducting material with the applied power, position, and temperature simultaneously. The wave penetration effects are rigorously included using the features of the three-dimensional finite-difference time-domain approach.

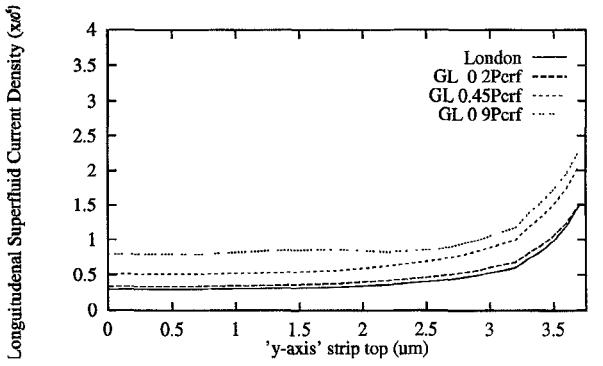

Fig. 16. Normalized longitudinal super fluid current density at the top surface of the HTS strip at different applied power levels.

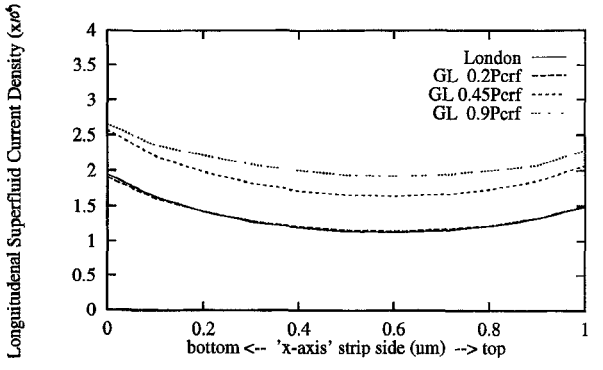

Fig. 17. Normalized longitudinal super fluid current density at the side surface of the HTS strip at different applied power levels.

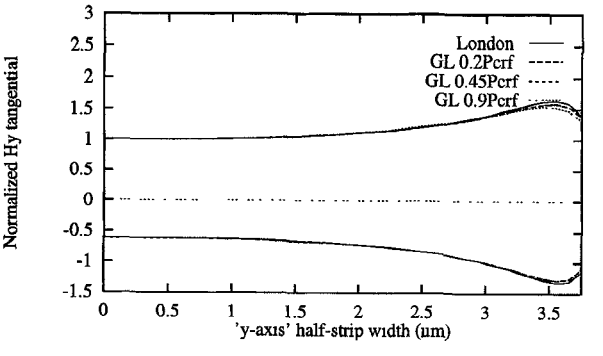

Fig. 18. Normalized tangential magnetic field intensity distribution at the top and bottom surface of the HTS strip at different applied power levels.

The nonlinearity in the HTS is modeled by the GL equations. The super fluid electron density is calculated at different levels of applied power. The maximum power for the HTS strip is predicted for the microstrip line. Numerical results show that a change in the phase velocity of the wave propagating along the line of about 1.5% occurs as the applied power reaches 0.9 of the maximum rf power. The corresponding increase in the attenuation is dramatic. It increased 170 times compared to the low power case. The effect on the electromagnetic field distribution is pronounced near the edge of the HTS strip. The super fluid current density distributions change

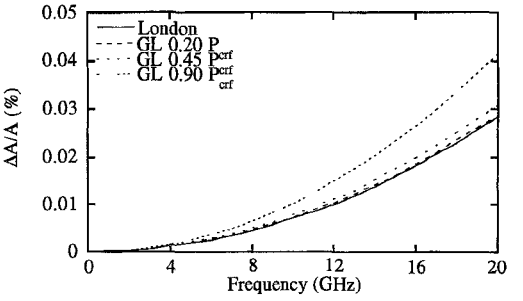

Fig. 19. Fractional change in the amplitude of the frequency spectrum of the output pulse w.r.t. the dc component at different applied power levels.

dramatically with the applied field. The change in the frequency spectrum is successfully depicted. The linear London model underestimates the field penetration inside the HTS material. It also overestimates the current crowding effects. Thus, the nonlinearity associated with the HTS material is successfully modeled and studied. Application of this complete three-dimension time-domain nonlinear simulator on different microwave and millimeter-wave devices will be presented in a later publication.

REFERENCES

[1] S. M. El-Ghazaly, R. B. Hammond, and T. Itoh, "Analysis of superconducting microwave structures: Application to microstrip lines," *IEEE Trans. Microwave Theory Tech.*, vol. 40, no. 3, pp. 499–508, 1992.

[2] J. M. Pond, C. M. Krowne, and W. L. Carter, "On the application of complex resistive boundary conditions to model transmission lines consisting of very thin superconductors," *IEEE Trans. Microwave Theory Tech.*, vol. 37, no. 1, pp. 181–189, 1989.

[3] D. Nghiem, J. T. Williams, and D. R. Jackson, "A general analysis of propagation along multiple-layer superconducting stripline and microstrip transmission lines," *IEEE Trans. Microwave Theory Tech.*, vol. 39, no. 9, pp. 1533–1564, 1991.

[4] H. Lee and T. Itoh, "Phenomenological loss equivalence method for planar quasi-TEM transmission lines with a thin normal conductor or superconductor," *IEEE Trans. Microwave Theory Tech.*, vol. 37, no. 12, pp. 1904–1909, 1989.

[5] T. E. van Deventer, P. B. Katehi, J. Y. Josefowicz, and D. B. Rensch, "High frequency characterization of high-temperature superconducting thin film lines," in *IEEE MTT-S Int. Microwave Symp. Dig.*, 1990, pp. 285–288.

[6] O. K. Kwon, B. W. Langley, R. F. Pease, and M. R. Beasley, "Superconductors as very high-speed system-level interconnects," *IEEE Electron Device Lett.*, vol. 8, no. 12, pp. 582–585, 1987.

[7] L. Lee, S. Ali, W. Lyons, D. Oates, and J. Goettee "Analysis of superconducting transmission line structures for passive microwave device applications," *IEEE Trans. Appl. Superconduct.*, vol. 3, no. 9, pp. 2782–2787, 1992.

[8] M. A. Megahed and S. A. El-Ghazaly, "Finite difference approach for rigorous full-wave analysis of superconducting microwave structures," in *IEEE Microwave Theory Tech.-S Int. Microwave Symp. Dig.*, 1993, pp. 808–811.

[9] G. L. Matthaei and G. Hey-Shipton, "Concerning the use of high-temperature superconductivity in planar microwave filters," *IEEE Trans. Microwave Theory Tech.*, vol. 42, no. 7, pp. 1287–1294, 1994.

[10] M. A. Megahed and S. M. El-Ghazaly, "Analysis of waveguides with nonlinear material: Applications to superconductor microstrip lines" in *24th Europ. Microw. Conf. Symp. Dig.*, 1994, pp. 502–506.

[11] C. Kuo and T. Itoh, "An iterative method for the nonlinear characterization of the high T_c superconducting microstrip line," in *21th Eur. Microwave Conf. Symp. Dig.*, 1991, pp. 655–660.

[12] Y. Liu and T. Itoh, "Characterization of power-dependent high-T_c superconductor microstrip line by modified spectral domain method," *Radio Sci.*, vol. 28, no. 5, pp. 913–918, 1993.

[13] C.-W. Lam, D. M. Sheen, S. M. Ali, and D. E. Oates, "Modeling the nonlinearity of superconducting strip transmission lines," *IEEE Trans.*

Appl. Superconduct., vol. 2, no. 2, pp. 58–65, 1992.
[14] J. J. Xia, J. A. Kong, and R. T. Shin, "A macroscopic model of nonlinear constitutive relations in superconductors," *IEEE Trans. Microwave Theory Tech.,* vol. 42, no. 10, pp. 1951–1957, 1994.
[15] F. London, *Super fluids.* New York: Wiley, vol. 1, 1950.
[16] R. D. Parks, *Superconductivity* (in two volumes). New York: Marcel Dekker, 1969.
[17] M. R. Beasley, "High-temperature superconductive thin films," *Proc. IEEE,* vol. 77, no. 8, pp. 1155–1163, 1989.
[18] L. C. Gupta and M. S. Multani, Eds., *Selected Topics in Superconductivity,* vol. 1 of *Frontiers in Solid State Sciences.* New York: Nova, 1991.
[19] M. A. Megahed and S. M. El-Ghazaly, "Analysis of anisotropic high temperature superconductor planar structures on sapphire anisotropic substrates," *IEEE Trans. Microwave Theory Tech.,* vol. 43, no. 8, 1995.
[20] X. Zhang and K. Mei, "Time-domain finite difference approach to the calculation of the frequency-dependent characteristics of microstrip discontinuities," *IEEE Trans. Microwave Theory Tech.,* vol. 36, no. 12, pp. 1775–1787, 1988.
[21] X. Zhang, J. Fang, K. Mei, and Y. Liu, "Calculations of the dispersive characteristics of microstrip by the time-domain finite difference method," *IEEE Trans. Microwave Theory Tech.,* vol. 36, no. 2, pp. 263–266, 1988.
[22] A. Taflove and M. Browdin, "Numerical solution of steady-state electromagnetic scattering using time-dependent Maxwell's equations," *IEEE Trans. Microwave Theory Tech.,* vol. 23, no. 8, pp. 623–630, 1975.
[23] K. S. Yee, "Numerical solution of initial boundary problems involving Maxwell's equations in isotropic media," *IEEE Trans. Antennas Propagat.,* vol. 14, no. 1, pp. 302–307, 1966.
[24] J. P. Berenger, "A perfectly matched layer for the absorption of electromagnetic waves," *J. Comp. Phys.,* vol. 114, no. 1, pp. 185–200, 1994.
[25] D. B. Davidson, "A parallel processing tutorial," *IEEE Trans. Antennas Propagat. Mag.,* vol. 32, no. 2, pp. 6–19, 1990.
[26] C. E. Reuter, R. M. Joseph, E. T. Thiele, D. S. Katz, and A. Taflove, "Ultrawideband absorbing boundary condition for termination of wave guiding structures in FD-TD simulations," *IEEE Microwave Guided Lett.,* vol. 4, no. 10, pp. 334–346.
[27] A. King, "Massively parallel solutions of complex electromagnetic problems," *Electromagnetic Code Consortium Symp. Proc.,* 1992, pp. 96–97.
[28] L. Lee, S. Ali, and W. Lyons, "Full-wave characterization of high-T_c superconducting transmission lines," *IEEE Trans. Appl. Superconduct.,* vol. 2, no. 9, pp. 49–57, 1992.
[29] T. Van Duzer and C. W. Turner, *Principles of Superconductive Devices and Circuits.* New York: Elsevier, 1981.
[30] O. G. Vendik and A. Y. Popov, "Can the bipolaron model be used for a description of microwave and infrared properties of a high-temperature superconductor?," *Philosophical Magazine B,* vol. 67, no. 6, pp. 833–845, 1993.

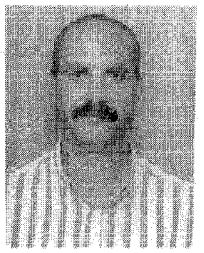

Mohamed A. Megahed (S'92–M'95) received the B.Sc. (Hons.) from the Military Technical College, Cairo, Egypt, and the M.Sc. from Alexandria University, Alexandria, Egypt, both in electrical engineering, and the Ph.D. degree in electrical engineering from Arizona State University, in 1995.

He is currently with the Telecommunications Research Center at Arizona State University. His research interests include microwave and millimeter-wave superconductor passive devices, microwave semiconductor devices and passive circuits, wave-device interactions, computational electronics and electromagnetics.

Dr. Megahed is a member of Sigma Xi and Eta Kappa NU.

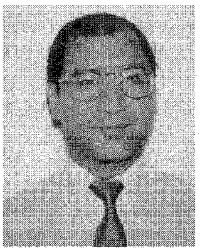

Samir M. El-Ghazaly (S'84–M'88–SM'91) received the B.Sc. degree in electronics and communications engineering (distinction, honors) in 1981, and the M.Sc. degree in 1984, both from Cairo University, Cairo, Egypt, and the Ph.D. degree, in electrical engineering, from the University of Texas at Austin, Texas, in 1988.

He joined Arizona State University as an Assistant Professor in August 1988, and became Associate Professor in 1993. He worked at several universities and research centers including the College of Engineering at Cairo University in Egypt, as a Teaching Assistant and Assistant Lecturer; the Centre Hyperfrequences et Semiconducteurs at Université de Lille I in France, where he worked on the simulation of submicron-gate MESFET's; University of Ottawa in Canada, where he worked on the analysis of E-plane circuits; the University of Texas at Austin as a Research Assistant and later as a Post-Doctoral Fellow; and at the NASA's Jet Propulsion Lab in Pasadena, CA, where he was a Summer Faculty Research Fellow working on millimeter-wave mixers. His research interests include microwave and millimeter-wave semiconductor devices and passive circuits, semiconductor device simulations, ultra-short pulse propagation, linear and nonlinear modeling of superconductor microwave lines, wave-device interactions, electromagnetics, and numerical techniques applied to monolithic microwave integrated circuits.

Dr. El-Ghazaly is a member of Tau Beta Pi, Sigma Xi, Eta Kappa Nu, and an elected member of Commissions A and D of URSI. He is on the editorial board of the IEEE TRANSACTIONS ON MICROWAVE THEORY AND TECHNIQUES as well as a member of the Technical Program Committee for the IEEE International Microwave Symposium since 1991. He was the Chairman of the IEEE-Waves and Devices Group, Phoenix Section and is the Chapter Funding Coordinator for IEEE MTT Society.